

**SONIC BOOM TESTING OF  
ARTIFICIALLY BLUNTED LEADING EDGE (ABLE) CONCEPTS  
IN THE NASA AMES AEROBALLISTIC RANGE**

Tim Tam \*

NASA Ames Research Center  
Moffett Field, CA

Stephen Ruffin +

Georgia Institute of Technology  
Atlanta, GA

Leslie Yates §

AerospaceComputing Inc.  
Los Altos, CA

Peter Gage £ and David Bogdanoff ££

Eloret Thermosciences Institute  
Sunnyvale, CA

John Morgenstern #

Lockheed Martin Skunk Works  
Palmdale, CA

**Abstract**

Sonic boom signatures and aerodynamic drag from several configurations in supersonic free-flight at near sea level conditions have been recorded at the NASA Ames Research Center aeroballistic range. Several different Artificially Blunted Leading Edge (ABLE) configurations were successfully designed, fabricated, and launched at Mach 2.0 and  $3 \times 10^6$  Reynolds number in the aeroballistic range to provide test data, outside the near-field, to assess their potential for reducing sonic boom on the ground for supersonic aircraft of the future. These results show that with some minor modifications, the Ames aeroballistic range serves as a viable test facility for high quality drag and sonic boom resolution on supersonic projectiles.

**Introduction**

Over the years, there has been great concern about the impact of supersonic jets flying over land and the sonic boom emanating from these vehicles. As the desire and need for time-critical business and leisure travel increases, supersonic passenger jets will play a key role in addressing the growing demand for high-speed air transportation.

However, supersonic aircraft create an undesirable and loud noise when the sonic boom emanating from the vehicle reaches the ground. Recent development of a new concept (ABLE) that provides sonic boom reduction with acceptable drag increase has led to the requirement of accurate experimental validation. In this paper, we will describe the process and challenges encountered in the design, fabrication, facility developments and enhancements, and successful sonic boom free-flight testing of the ABLE concept in an aeroballistic range.

\* Assistant Branch Chief, Associate Fellow, AIAA.

+ Associate Professor, Associate Fellow, AIAA.

£ Senior Research Scientist, Senior Member, AIAA.

££ Senior Research Scientist, Associate Fellow, AIAA.

§ Vice-President, Senior Member, AIAA.

# Senior Research Specialist, Member, AIAA.

	Conventional Design	Low - Boom Design
Bow Shock	Weak	Strong
Secondary Shocks	Strong and Multiple	Weak and Few
	Sharp Nose	Blunt Nose
Near Field		
Mid Field		
Ground	2 to 3 psf High Boom Low Drag	0.7 to 1.1 psf Low Boom High Drag

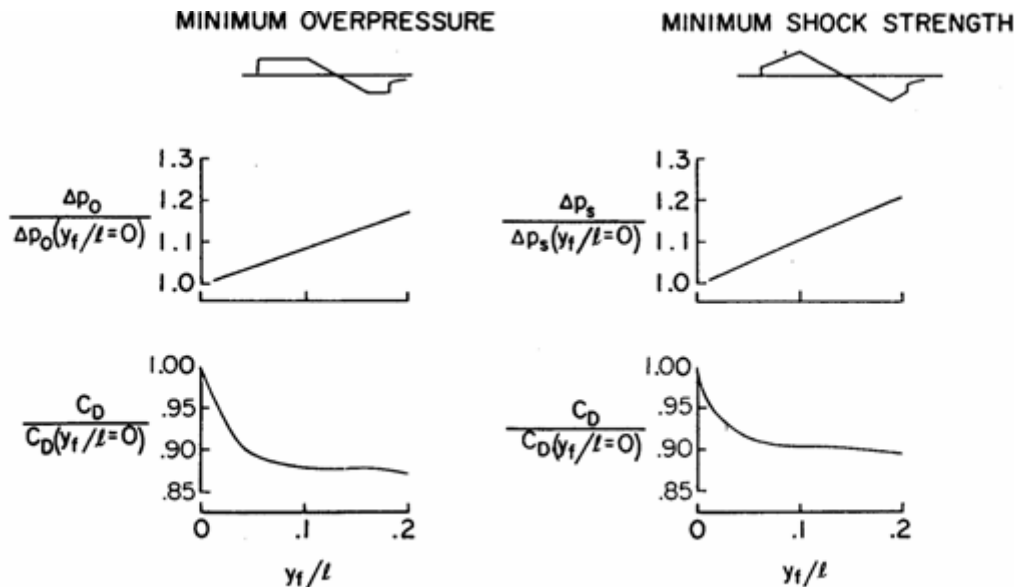
The low-boom - high drag paradox

**Figure 1. Blunt and sharp nose boom signatures (reprinted from Ref. 20)**

### Background

The most successful strategies utilized for minimization of sonic boom stems from evaluation of the Whitham F-function (Refs. 1-3). The F-Function is based on the cross-sectional area distribution and the lift distribution of the generating vehicle. Modified linearized theory and geometric acoustics are used to determine ground pressure signatures from the F-Function. Studies by Seebass and George (Ref. 4) and

Darden (Ref. 5) demonstrated that mid-field and far-field over-pressures are minimized when a significantly blunted nose is utilized on the vehicle. As illustrated in Fig. 1, when a blunt nose is utilized the subsequent compressions are weak, however for sharp-nosed vehicles subsequent compressions around the vehicle tend to be strong and coalesce in the far-field into a much stronger over-pressure relative to a blunt nose geometry. However, significantly blunted supersonic cruise vehicles have not been utilized because the wave drag becomes unreasonably high. The relationship between nose bluntness and boom characteristics has been validated with experimental studies in Refs. 5 and 6. The studies by Darden (Fig. 2) of vehicles with a relaxed level of nose bluntness clearly show that minimizing boom must be paid for by higher drag penalties. Optimization studies (Refs. 7-11) have sought to find an acceptable compromise for this low-boom high-drag paradox, but breakthroughs in design of aerodynamically efficient, low-boom vehicles require consideration of innovative approaches in vehicle design.



Estimated drag increments associated with configuration changes for sonic boom minimization:  $M = 2.7$ ;  $h = 18,288$  m (60,000 ft);  $w = 272,155$  kg (600,000 lb).

**Figure 2. Variations of over-pressures and drag with nose bluntness. Note:  $y_f = 0$  corresponds to flat-face nose. (reprinted from Ref. 7)**

## **Artificially Blunted Leading Edge (ABLE) Approach**

The proposed new concept generates the strong, normal bow shock needed for boom minimization but does so while experiencing significantly lower total drag than a conventional blunted geometry. When a conventional blunted geometry is in supersonic flight, a strong normal shock is generated yielding high surface pressure in the stagnation region and thus high wave drag. It is proposed that a hollow channel be constructed at the nose of the vehicle and along the wing leading edges. Freestream air is allowed to flow passively through the channel and is exhausted in a rearward facing direction as shown in Fig. 3. This can be accomplished by exhausting the flow through the rear of the body (i.e. “straight channel” configuration) or near the leading edge (i.e. “cowl” configuration). When the channel concept is utilized, the vehicle surface which experiences most of the high pressure on a conventional blunted geometry is removed and thus use of the channel leads to significantly lower wave drag. If the channel is sufficiently small, a choked flow condition exists in which a strong normal shock rests in front of the nose and the flow enters the channel subsonically. The choked channel generates an “effective blunt body” and the overall flow structure is similar to that near a conventional blunted geometry. A geometry employing this approach is said to have an Artificially Blunted Leading Edge (ABLE).

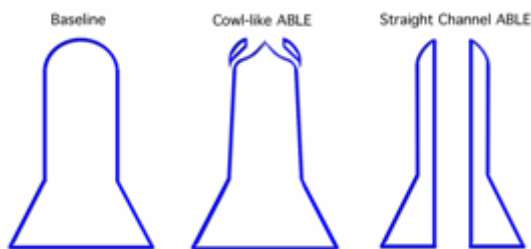


**Figure 3. Cross sectional views of some ABLE concept applications to vehicle nose.**

## **Numerical Studies**

A numerical study of the channel ABLE has been performed for several airfoils (Refs. 12, 13) and axisymmetric sphere-cone geometries (Ref. 18). Navier-Stokes predictions of the flow were performed using GASP (Ref. 15), a multi-block finite volume solver, and it is found that use of a channel significantly improves aerodynamic performance relative to more conventional, blunted geometries. For example, when 5% thick diamond airfoils with leading edge radii of 5mm are investigated, it is found that total drag (including skin friction) decreases by over 30% when compared with blunted airfoils without channels for flight at  $M = 2.4$ . Although skin friction drag increases, there is a net reduction in total drag due to a large reduction in wave drag.

Additional calculations and experimental studies of axisymmetric nose geometries also demonstrate that use of a channel leads to significantly improved aerodynamic efficiency relative to conventional, blunted geometries. To experimentally validate the predictions at one freestream condition, “straight-channel” ABLE and solid sphere-cone models (Initial Aeroballistic Range Tests section) were flown in the NASA Ames Research Center Aeroballistic Range.

## **Limitations of Wind Tunnel Sonic Boom Measurements**

Previous wind tunnel tests have revealed a difficulty in getting accurate sonic boom measurements from a wind tunnel environment. Geometry very similar to the solid forebody shown in Fig. 4 was measured for sonic boom in Ref. 16. Fig. 5 shows the rounded wind tunnel measurements versus the predicted strong bluntness shock, followed by a constant pressure region, an expansion from the base, and finally, a recompression from the

sting. In Ref. 17, the cause of this disparity was attributed to vibration of the model, relative to the flow, resulting in an averaging of the actual pressure change (Fig. 6.)

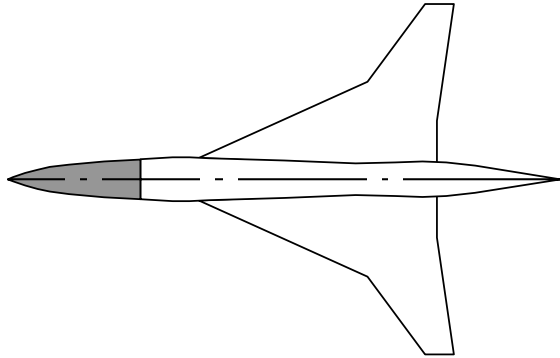


**Figure 4. Aeroballistic sharp nose model in relation to the rest of the supersonic aircraft.**

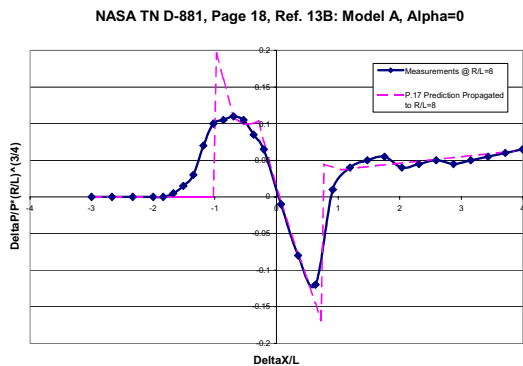


**Figure 5. Wind tunnel measurements are rounded compared to the prediction.**

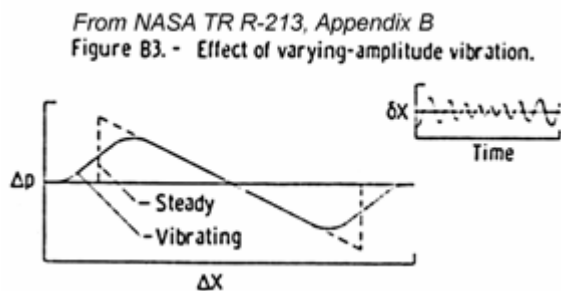


**Figure 6. Typical wind tunnel vibration and turbulence cause the shock rounding in shown in figure 5.**

While larger wind tunnel models could reduce this averaging effect, an aeroballistic range presents an extremely steady freestream environment for accurate shock resolution (among other things like low turbulence for laminar flow and high Reynolds number sea level density.) Accurate shock resolution in the nose region is very important for sonic boom because any error in the minimum F-function at the nose proportionally effects the shock strength, whereas small errors in other locations often disappear in the propagation to the ground. Previous investigations have shown that the aeroballistic range is a suitable environment to record sonic boom signature of small axisymmetric models (Ref. 24) with minimal noise.

### Initial Aeroballistic Range Tests

Aerodynamic performance parameters,  $C_D$ ,  $C_L$ , and  $L/D$  as a function of angle of attack were obtained for the straight-channel ABLE and baseline solid sphere-cone configurations using trajectory based analysis from experimental shadowgraphs and time of arrival information. The  $M = 2.4$  tests were conducted (Fig. 7, Ref. 19) at the NASA ARC Aeroballistic Range and computational fluid dynamics (CFD) analysis, provided by Georgia Institute of Technology, successfully predicted the drag, predominant flow structures, especially the base flow barrel shock and Mach disk features, consistent with experimental results.

The data confirmed drag reduction, lift increase, and  $L/D$  performance enhancement trends predicted for ABLE channel geometries. The measured 35% nominal  $L/D$  performance increase at small angles of attack is considered very significant. The drag reduction due to the channel for these axisymmetric bodies was approximately 10%. This percent drag reduction is smaller than that described earlier for 2-D bodies. This is

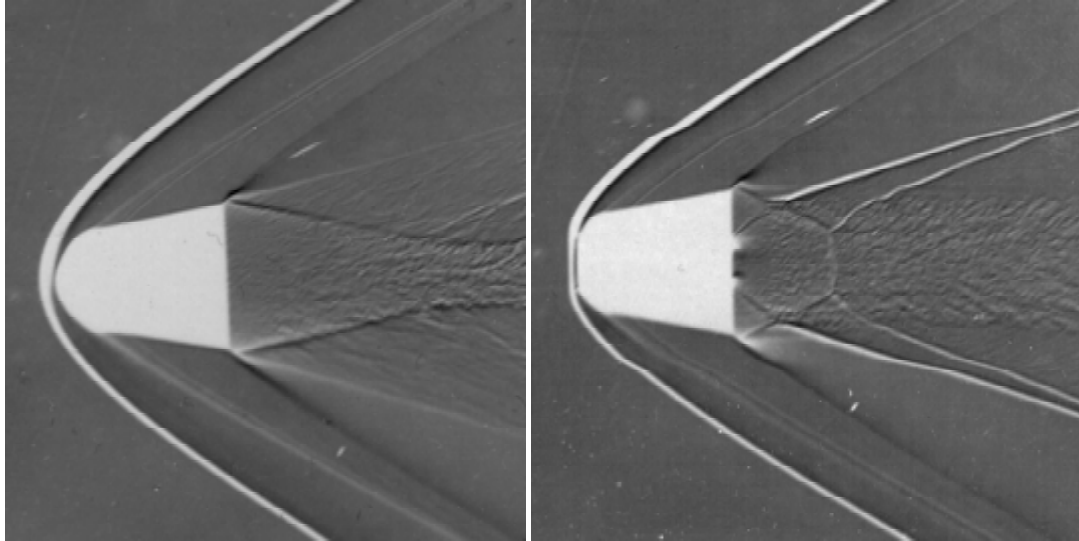


**Figure 7. Aeroballistic range shadowgraphs of baseline solid sphere/cone (left) and ABL models (right),  $M = 2.3$ ,  $p = 1 \text{ atm.}$ , base dia. = 2.54 cm, length = 2.95 cm.**

true because the wave drag due to bluntness is smaller for axisymmetric bodies compared to 2-D geometries, and it is the wave drag due to bluntness that ABL reduces.

Next, the effort was focused on modifying a single aeroballistic range station and equipping it with a pressure transducer at the test section wall to measure sonic boom signatures for ABL and baseline configurations. Different transducers and housing port designs were investigated (Experimental Set-Up section) in an effort to minimize noise in the recorded sonic boom signature. As shown in Fig. 8, a 12% bow wave boom reduction was measured for the ABL straight-channel configuration

These initial aeroballistic range tests experimentally confirmed the numerically predicted drag reduction potential of the ABL concept for blunt sphere-cones and demonstrated that the ARC aeroballistic range had strong potential as a sonic boom test bed. A follow on collaborative effort between Langley Research Center (LaRC), Lockheed Martin Skunk Works (LMSW), Georgia Institute of Technology (GIT), and Ames

Research Center (ARC) was brought together to apply ABL to sonic boom minimized aircraft. To achieve greater sonic boom reductions, ABL was applied to a Seebass and George (Ref. 4) minimized F-function. Darden’s method (Ref. 14) was used to determine the area distribution necessary for a minimized F-function. To determine if applying “ABL bluntness” helps circumvent the low boom-high drag paradox described in Figure 1, both accurate drag and boom measurements were needed.

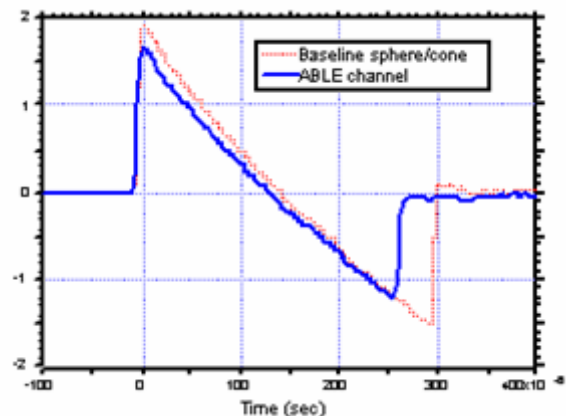


**Figure 8. Experimental N-wave signatures for solid sphere/cone and ABL geometries,  $M = 2.3$ ,  $p = 1 \text{ atm.}$ ,  $H/L \sim 40$ .**

Quantifying ABLE's benefit to aircraft required changes in design approach from the channel-based concepts described previously. A "cowl-like" ABLE geometry was deemed more practical for a transport aircraft application, due to expected difficulties in integrating a channel through a significant portion of an aircraft's length. In order to quantify ABLE's effect, geometry simplifications were made. Since bluntness is only necessary at the leading edge or nose of a minimized F-function, only the forebody of the sonic boom minimized aircraft was needed to assess the ABLE effect. To make boom and drag differences easily comparable, the same length and minimized area distributions were used for all forebodies, with the only difference being 3 different ABLE cowl geometries and a solid baseline. The baseline forebody's relation to an aircraft is shown in Fig. 4. A total of four designs were investigated. These designs included a solid geometry with a sharp leading edge and three ABLE designs with different cowl regions. The designs tested were: (1) solid nose (baseline), (2) long cowl, (3) short cowl 1, and (4) short cowl 2. In this paper, sample results from the solid nose model will be shown to demonstrate the data reduction process and the quality of data from the aeroballistic range.

### **Experimental Set-Up**

The NASA ARC aeroballistic ranges have for years conducted high-speed aerodynamic tests and contributed to various agency programs (Refs. 21, 22). Recently, after a dormant period of about seven years, ARC embarked upon a refurbishment project to reactivate the Hypervelocity Free Flight Aerodynamic Facility (HFFAF), NASA's only aeroballistic range. In support of the current sonic boom testing, the facility was instrumented to obtain sonic boom signatures from free-flight projectiles. The models encased in a sabot for protection from the hot gases and g-loads

during the launch were propelled from a 4.4 cm diameter powder gun into a 16 station, 23 m long test section. The stations are 1.5 m apart and equipped with an orthogonal shadowgraph system using spark gap white light sources and Kerr cell shutters. Shadowgraphs are obtained at each station and scanned into image files and digitally reduced, providing axial location to within 0.0025 cm (0.001") and model orientation (angle of attack and yaw) to within 0.5 degree. A data reduction routine CADRA (Ref. 23) is used to provide aerodynamic data including pitch damping coefficients. Improvements to the facility instrumentation were required to obtain accurate sonic boom measurements.

### **Instrumentation for Sonic Boom Measurement**

In the 1970's ARC performed an experiment (Ref. 25) in the aeroballistic range to investigate the effects of sonic boom overpressures in water using shadowgraphs and a pressure transducer instrumented in a water tank. The current effort required an accurate time history of sonic boom signatures along the wall of the test section and the overall drag as the models flew by. The need to assess angle of attack affects meant that multiple stations be instrumented to gather data on sonic boom signatures without altering the existing shadowgraph stations. In order to perform the measurements, nine of the 16 side stations along the 23 m aeroballistic range test section were modified and instrumented with pressure ports and transducers to record pressure signatures of models in free-flight.

After investigating different designs and mounting techniques, it was concluded that PCB transducers flush mounted to the facility wall provided the best option. Flush mounting minimized the noise or "ringing" in the signal compared with data from the transducer that was installed set back from the test section

wall. The PCB transducers also provided the best combination of adequate response time and price. Thirteen model 113A21 quartz crystal piezoelectric pressure transducers were installed in the walls of aeroballistic range test section. The sensitivities of these transducers are  $\sim 25$  mV/psi. Transducers were installed at a 45-degree azimuth location (top left looking from the gun muzzle) at stations 1, 3, 5, 7, 9, 10, 12, 14 and 16. Four additional transducers were installed at station 5 at the 0, 90, 180 and 270-degree azimuth locations. These transducers were mounted in carbon steel transducer holders with a body diameter of 3.8 cm, flange diameter of 8.3 cm and depth of 3.8 cm. The transducer holders at the 45-degree azimuth locations were mounted directly in the steel wall of the range. The other transducer holders at station 5 were mounted in aluminum plates, which replaced the observation windows at this station.

The transducers were connected to two PCB Model 483A, 12-channel amplifiers, which were located in the range room. PCB calibrated all the amplifiers and the transducers prior to the test series. RG-58U cables from the outputs of the Model 483A amplifiers were connected to LeCroy Model 8100 amplifiers located in a trench under the range room. These amplifiers were set at a gain of 50. From the Model 8100 digitizers, cables were run to four LeCroy Model 6810 digitizers of the aeroballistic range data acquisition system controlled by a computer. These four digitizers provide a total of 16 data channels, sufficient for the 13 sonic boom pressure transducers plus one other transducer to allow the recording of the powder pressure history in the gun used to launch the models. The Model 6810 digitizers are 12-bit units and were operated at 500 kHz, a sensitivity range of  $-5$  V to  $5$  V and with a 64 K record length. The digitizers were triggered off the pulse used to fire the model launch gun. The RMS noise levels at the digitizers (checked just

before each run) are typically  $\sim 10$  mV, while a typical sonic boom N-wave has a peak-to-peak amplitude of 2 V to 3 V. Thus, if the peak-to-peak noise level is estimated to be  $\sim 30$  mV, the signal-to-noise ratio is 70 - 100.

### Model Design and Fabrication

GIT and LMSW supplied the outer mold lines for the models and ARC conducted detailed design to ensure safe and stable flight in the ballistic range. Additional model design objectives were determined by the launch velocity and flight stability of the projectile. A Mach = 2.0 test condition for the 7.62 cm long models was chosen to match the vehicle's design cruising velocity.

The first design requirement was to have a statically stable model. A detailed model design was constructed on a Pro-E platform where the mass properties could be easily manipulated and tailored to keep the center of gravity well ahead of the predicted center of pressure (from CFD results) for a large static margin. This particular model designed required use of two different materials with a dense, stainless steel forebody and relatively light, magnesium afterbody. Fig. 9 shows a design drawing of the solid nose (baseline) model

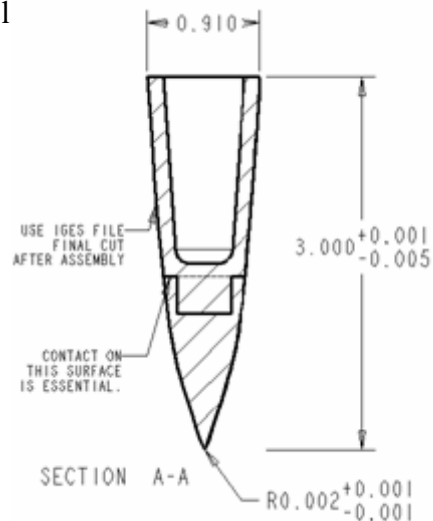


**Figure 9. Sharp nose model dimensions.**

For this model design, stability requirements necessitated that the afterbody be hollowed out from the base and the material split line shifted well forward. The steel and magnesium used to in the fore and afterbody respectively, provided a large density ratio while maintaining machineability. Figure 10 shows a sample of the CFD results used in the model design process. The models were designed to have approximately 1.0 - 1.5 cycles of motion in the pitch plane within the test section. Although not a major factor in these particular tests, the amplitude of model motion (pitch and yaw) is especially critical in tests where accurate measurement of other aerodynamic coefficients such as pitch and yaw damping are desired.

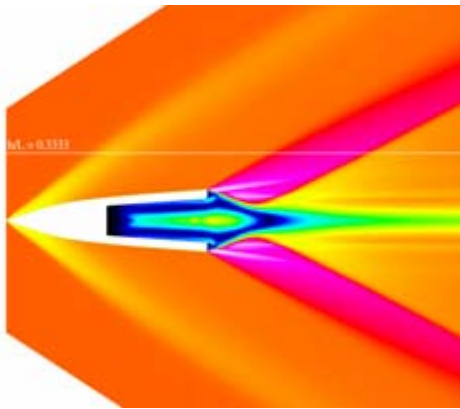


**Figure 10. Sample CFD results of the sharp nose model.**

Another key design requirement was that the model internal geometry design be both machineable and robust enough to survive the gun launch loads. The ABLE designs called for internal channels that allow air to pass through the nose region of the model. After discussing several approaches with ARC facility and fabrication shop personnel, it was decided that a pin and strut design (Fig. 11) was the most feasible. First, the model forebody and afterbody was fabricated and hollowed out and attached together. The model forebody (steel) surface was then "etched" with footprints to accommodate the

struts using an electric discharge manufacturing (EDM) process. Once the struts were temporarily secured in the



**Figure 11. ABLE model parts: cowl nose cap, forebody, and struts.**

footprints on the forebody, a spherical nose cowl was placed over the forebody, strut, and pin combination. Holes were then drilled through the cowl surface, struts and into model forebody. Shear pins were then inserted into the holes to strengthen the entire assembly and the cowl surface was polished to maintain the surface roughness requirements. The Pro-E platform facilitated model design by permitting rapid variation of split line location, internal geometry features, and critical mass properties such as center of gravity and moment of inertia. The afterbodies were similar for all models, so a standard afterbody was quickly customized for each shape variation.

The parts files were electronically sent to the ARC fabrication shop, which in turn were used to electronically generate numeric machining tool paths. This process contributed significantly increased model accuracy and reduced turnaround time. Multiple models were built employing each of the four designs and a summary of the conditions for the 14

shots fired are shown in Table 1. For each of the 14 shots, the pressure transducers recorded pressure vs. time as the model crossed each of the nine-instrumented stations.

### Data Reduction

The orthogonal stations provided shadowgraph pictures (Fig. 12) that were scanned into digital images and interpreted for drag results using the CADRA program to provide model location, velocity, and orientation. This data is then combined with readings from the facility counters at each station to obtain aerodynamic coefficients. Sonic boom data signatures were correlated with flight Mach number, orientation, and distance from flight path. These correlated results were then extrapolated to the far field.

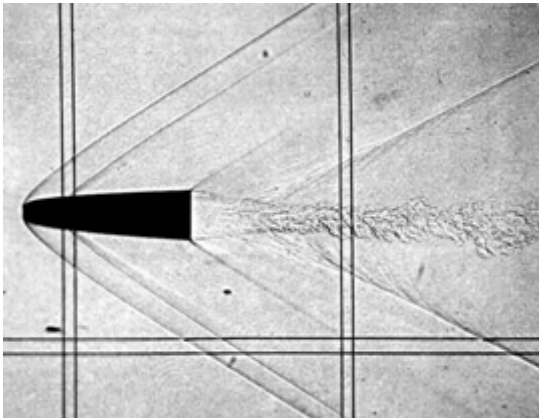


**Figure 12. Typical shadowgraph from one of the ABLE model tests.**

### Correlating Sonic Boom and Model Orientation Data

Because the models decelerated in flight and followed a trajectory that was not perfectly straight, each of the transducer measurements corresponded to a different local flight Mach number and a different flight path angle and distance relative the transducer surface. Correlating the shadowgraph data to the sonic boom signatures allowed corrections to the pressure signatures such as Mach number,

trajectory, and angle of attack differences. For Shot 2183 of the sharp nose test, the Mach number dropped from 2.075 to 1.989 as the model proceeded from station 1 to 16 and the flight path angle relative to the transducers remained less than 0.6 deg. The distance from the transducers ranged from 7.1 to 8.8 body lengths from the model. Because the sonic boom is sensitive to the Mach number and angle of attack, only shots with nearly the same average Mach number and low flight path angles relative to the transducers were selected for far-field boom extrapolation.

### Extrapolating Data to the Far-Field

Each recorded pressure signature for the selected shots was extrapolated to the far-field using the NFBOOM code developed at NASA Ames Research Center. A sonic boom signature recorded from the aeroballistic range for a forebody model is shown in Fig. 13.

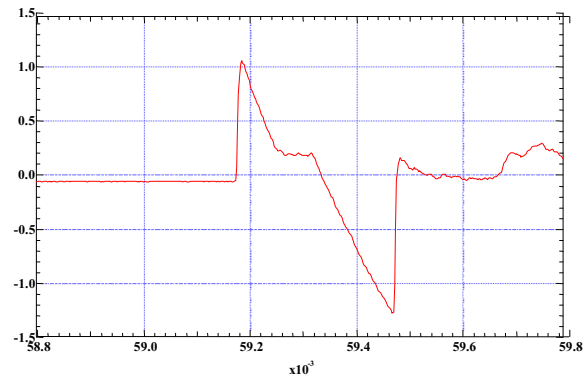


**Figure 13. Forebody model sonic boom results. (Signal/volt vs. Time/sec)**

The NFBOOM code is based on the waveform method of Thomas (Ref. 26) but has been modified to perform extrapolation through non-uniform atmospheres when a mid- or far-field static pressure distribution is specified. The NFBOOM code also scales the specified mid- or far-field signature obtained from a small model to the signature produced by much larger flight geometry. For each of the

transducer signatures, the local values of Mach number and local distance from the transducer was utilized. The experimental models were scaled up from a length of 7.6 cm to 3 m to match the nose dimensions of a small supersonic aircraft. The extrapolated signatures from NFBOOM reported in the present study correspond to a flight altitude of 15 km.

The NFBOOM extrapolated shock overpressures based on the measured transducer signatures were then plotted as a function of the local flight path angles relative to the transducer. A least squares fit was then performed so that the effect of relative angle on boom overpressure was obtained for each shot. Finally, the ground overpressure corresponding to a relative flight path angle of 0 deg. was determined for each geometry

### Sample Results

The initial pressure spike in Fig. 13 from the nose is followed by a flat, weak compression region, corresponding to the slow area growth behind the nose, and finally, a strong expansion due to the base area. In a full configuration test, the base area expansion would be replaced by the rest of the boom-minimized aircraft. Drag results shown in Fig. 14 indicate the variation of  $C_{D0}$  as a function of Mach number. The data points in Fig. 14 represent drag values from shadowgraph measurements, which were reduced individually for each shot employing a linear aerodynamic coefficients data reduction routine. Multiple data sets were reduced using nonlinear coefficients and are represented by the line fits. Uncertainty in the drag measurements obtained is less than 1% when compared with predictions. Fig. 15 shows a comparison between a forebody sonic boom measurement and its design target. On this model, there was a mismatch in the far-field based target and the measured pressure

distribution. Even though the mismatch is small, Fig. 16 shows that propagation of the measured distribution to the ground results in 9% greater front shock strength than the target. The design methodology was updated to more precisely achieve target distributions in later designs.

**( $C_{D0}$  vs. Mach Number)**

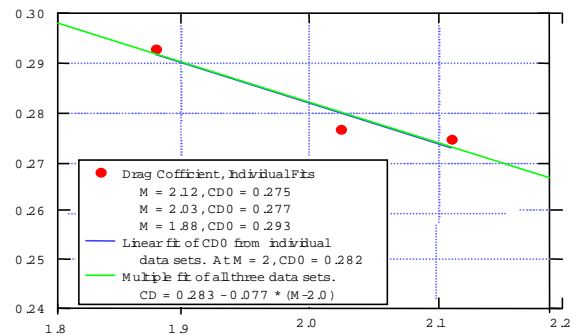


**Figure 14. Sharp nose model drag results.**

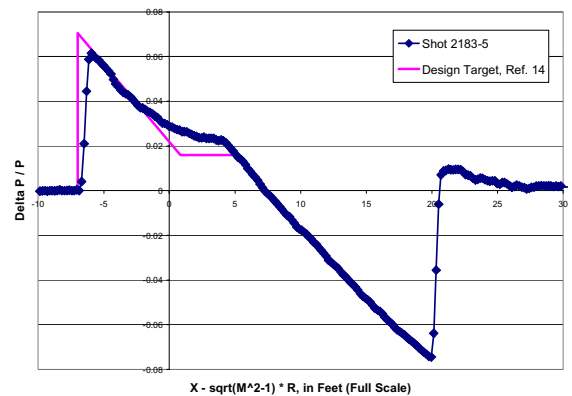


**Figure 15. Slight mismatch in forebody measured sonic boom was captured by high resolution of aeroballistic range.**

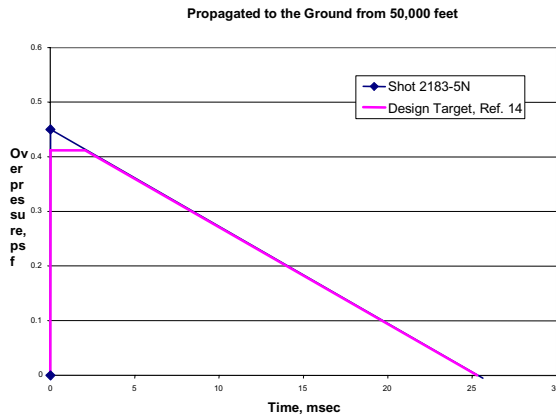


**Figure 16. Mismatch is predicted to result in a 9% greater shock strength—This resolution helped develop a more precise design method.**

### Concluding Remarks

Modifications were made to the NASA Ames aeroballistic range to enable sonic boom testing. The quiescent freestream and free-flight test conditions of the aeroballistic range environment are desirable and resulted in high-resolution pressure traces with acceptable noise levels. The model design, fabrication, testing, data acquisition, and data reduction methodologies are in place to investigate various axisymmetric configurations suitable for component testing. The combination of the rapid model design, electronic document exchange with the fabrication shop, instrumentation development that enhanced facility capability, responsive facility turnaround, and computerized data reduction with digital images were critical

factors that it made it possible to meet a very aggressive schedule. The entire process from outer mold line release, model design, fabrication, facility preparation, testing, data analysis, to final program review of the 14 model test program was completed in six months. This new capability in combination with the established aerodynamic testing methods makes the aeroballistic range a uniquely viable test bed to investigate sonic boom. Increasing model complexities to include vehicles with fins or wings would allow free-flight testing, outside the near-field, to screen vehicle concepts at a small fraction of the cost of flight tests.

### Acknowledgements

The authors would like to thank James Scott and Lee Morgan for their insightful discussions and excellent craftsmanship during the design and fabrication stages of these extremely high precision models. The responsiveness of the aeroballistic range staff, Charles Cornelison, Don Holt, Don Bowling, Robert Kruse, and Johnathan Brown, played a key role in enabling the test program to meet its objectives and schedule. Initial aeroballistic range tests, led by Mark Newfield, were vital to the development of instrumentation used in these tests. CFD support provided by Grant Palmer, James Reuther, and Shannon Wilson is gratefully acknowledged. The graphic support provided by Jay Nuez is also gratefully acknowledged. Finally, special thanks to Peter Coen and Tom Hartmann for their support of these tests.

**Table 1.**

Run Number	Model	Mach Number (Sta. 1-16 avg.)	Pressure (mm)	Temp. (°C)
2179	Long Cowl	2.40	764.3	25.8
2180	Long Cowl	1.90	765.1	25.1
2181*	Long Cowl	2.03	765.5	24.4
2182*	Long Cowl	2.03	765.6	25.7
2183*	Sharp Nose	2.03	765.1	24.6
2184	Sharp Nose	2.11	765.8	24.3
2185*	Sharp Nose	1.87	767.2	24.4
2186	Sharp Nose	2.09	759.1	24.4
2187	Short Cowl 1	2.11	762.2	22.7
2188	Short Cowl 1	1.93	766.1	22.9
2189*	Short Cowl 1	2.01	764.5	23.3
2190*	Short Cowl 2	2.02	764.1	24.3
2191	Short Cowl 2	1.98	765.5	23.7
2192	Short Cowl 2	1.92	765.5	23.1

\* Shot Utilized for Far-Field Boom Extrapolation

### References

- Whitham, G.B., "The Flow Patter of a Supersonic Projectile," *Communications on Pure and Applied Mathematics*, Vol. V., pp. 301-348, 1952.
- Carlson, H.W., and Maglieri, D.J., "Review of Sonic Boom Generation Theory and Prediction Methods," *Journal of Acoustical Society of America*, Vol. 51, pp. 675-685, 1972.
- Middleton, W.D., and Carlson, H.W., "A Numerical Method for Calculating Near-Field Sonic-Boom Pressure Signatures," NASA TN D-3082, 1965.
- Seebass, R., and George, A.R., "Sonic Boom Minimization," *Journal of the Acoustical Society of America*, Vol. 51, No. 2, Part 3, pp. 686-694, 1972.
- Mack, R.J., and Darden, C.M., "Wind Tunnel Investigation of the Validity of a Sonic-Boom-Minimization Concept," NASA TP-1421, 1979.
- Carlson, H.W., Mack, R.J., Morris, O.A., "A Wind Tunnel Investigation of the Effect of Body Shape on Sonic-Boom Pressure Distributions," NASA TN D-3106, November 1965.
- Darden, C.M., "Sonic Boom Theory: Its Status in Prediction and Minimization," *Journal of Aircraft*, Vol. 14, No. 6, pp. 569-576, 1977.
- Haglund, G.T., "HSCT Designs for Reduced Sonic Boom," AIAA Paper 91-3103, AIAA Aircraft Design Systems and Operations Meeting, September 1991.
- Mack, R.J., Needleman, K.E., "A Methodology for Designing Aircraft to Low Sonic Boom Constraints," NASA TM 4246.
- Yoshida, K., and Tokuyama, A., "Improving the Lift to Drag Characteristics of Low Boom Configuration," AIAA Paper 92-4218, August 1992.

11. Yoshida, K., "Experimental and Numerical Study for Aerodynamics of Low Boom Configuration," AIAA Paper 94-0052, Aerospace Sciences Meeting, January 1994.
12. Ruffin, S.M., and Gupta, A., "Supersonic Channel Airfoils for Reduced Drag," AIAA Paper 97-0517, Aerospace Sciences Meeting, January 1997.
13. Gupta, A., Ruffin, S.M., "Optimal Artificially Blunted Leading Edge (ABLE) Airfoils for Hypersonic Performance Enhancement," *Journal of Spacecraft and Rockets*, Vol. 36, No. 4, pp. 499-506, July-August 1999.
14. Darden, C.M., "Sonic-Boom Minimization With Nose-Bluntness Relaxation," NASA TP-1348, January 1979.
15. Walters, R.W., et al, "GASP Version 3, The General Aerodynamic Simulation Program – User's Manual," Aerosoft, Inc., May 1996.
16. Carlson, H.W., "An Investigation of the Influence of Lift on Sonic-Boom Intensity by Means of Wind-Tunnel Measurements of the Pressure Fields of Several Wing-Body Combinations," NASA TN D-881, July 1961.
17. Carlson, H.W., "Correlation of Sonic-Boom Theory with Wind-Tunnel and Flight Measurements," NASA TR R-213, December 1964.
18. Gupta, A., Ruffin, S.M. and Newfield, M. "Aerothermodynamic Performance Enhancement and Design of Blunted Sphere-Cones using the ABLE Concept," AIAA paper 99-0897, January 1999.
19. Newfield, M. and Ruffin, S.M., "Validation of a Nose Channel Concept for Supersonic Drag Reduction," NASA TM-1999-112240, March 1999.
20. Brown, J.G., and Haglund, G.T., "Sonic Boom Loudness Study and Airplane Configuration Development," AIAA Paper 88-4467, September 1988.
21. Interieri, P.F., "Study of Stability and Drag at Mach Numbers from 4.5 to 13.5 on a Conical Venus-Entry Body," NASA TN D-2827, May 1965.
22. Sammonds, R.I, and Kruse, R.L., "Viking Entry Vehicle Aerodynamics at M = 2 in Air and Some Preliminary results Test Data For Flight in CO<sub>2</sub> at M = 11," NASA TN D-7974, June 1975.
23. Yates, L.A., "A Comprehensive Automated Aerodynamic Reduction System for Ballistic Ranges," WL-TR-96-7059, Wright Laboratory, Armament Directorate, October 1996.
24. Callaghan J.G., "A Feasibility Investigation Concerning the Simulation of Sonic Boom by Ballistic Models," NASA CR-603, October 1966.
25. Intrieri, P.F. and Malcom, G.N., "Ballistic Range Investigation of Sonic-Boom Overpressures in Water," AIAA Journal, Vol. 11, No. 4, pp. 510-516, April 1973.
26. Thomas, C.L., "Extrapolation of Sonic Boom Pressure Signatures by the Waveform Parameter Method," NASA TN D-6832, June 1972.